

Locally Scaled Self-Interaction Corrected Energy Functionals with Complex Optimal Orbitals

Jukka John,¹ Hlynur Guðmundsson,¹ Iðunn Björg Arnaldsdóttir,¹ Hannes Jónsson,^{1,*} and Elvar Örn Jónsson^{1,†}

¹*Science Institute and Faculty of Physical Sciences, University of Iceland, 107 Reykjavík, Iceland*

(Dated: January 28, 2026)

We present a fully variational locally scaled self-interaction corrected (SIC) energy functional using complex optimal orbitals. This represents an important milestone for fully variational SIC energy functionals, which have been shown to improve the prediction of the properties of atomic, molecular and solid state systems in general, in both ground and excited states. However, it depends on the system and property of the system whether it is beneficial to scale the SIC correction by a factor of one-half, which makes the application of SIC inconsistent. In the limit of a single electron the SIC exactly cancels the self interaction error, but overcorrects the error in regions of high density where there is large overlap between occupied orbitals. The newly implemented local scaling function, $z(\mathbf{r})$, which is based on an iso-orbital indicator derived from considering the kinetic energy density in the iso-electron and many electron case, naturally scales the SIC correction from $0 \leq z(\mathbf{r}) \leq 1$ in regions of high and low (isolated orbital) electron density. The locally scaled SIC framework is general and applicable to atomic, molecular and solid-state systems.

I. INTRODUCTION

Kohn–Sham density functional theory (KS–DFT) [1, 2] is the most widely used method for electronic structure calculations in materials science, chemistry, and nanotechnology. Despite its success, it has several shortcomings. In KS–DFT, a local or semilocal approximation to the exchange–correlation energy of the electron density is typically applied. This transforms the problem of N interacting electrons to a problem of three spatial variables which describe the total electron density. Therefore KS–DFT provides a feasible way to simulate systems with thousands of electrons. However, approximations to the true exchange–correlation energy introduce the so-called self interaction error (SIE) which comes from the partial cancellation of the self-coulomb and self-exchange correlation interaction of the electron with itself in the effective potential.

Due to the SIE, the description of localized electronic states in semiconductors and insulators is problematic, [3–8] the excitation energy of diffused (Rydberg) and valence electron states [9–13] are poorly described, the relative energies of s- and d-electrons in transition metal molecules [14, 15] are not balanced, leading to incorrect magnetic states, and bond energies of gas phase molecules are often greatly overestimated (e.g. O₂ which is off by 1 eV [16]) and absorption energy of ad-molecules and intermediates on solid surfaces in catalytic reactions [17] are too inaccurate for a quantitative prediction.

Perdew and Zunger proposed a procedure where the orbital-by-orbital SIE is subtracted from the total energy functional[18]. The resulting Perdew-Zunger self-interaction correction (PZ-SIC) energy functional tends to overcorrect the energetics of the base functional, and

scaling down the correction is necessary for a better estimate of orbital energies. [19–22] Empirical evidence suggests to include a scaling factor of $\frac{1}{2}$ ($\frac{1}{2}$ SIC) which was shown to work well for different types of systems and properties [6, 20, 23]. $\frac{1}{2}$ SIC has been applied to a wide range of systems, giving better agreement than local or semi-local KS–DFT energy functionals in calculations of the atomization energy of molecules, [24, 25] activation energy of chemical reactions, [16] electronic excitation energies [26] and band gaps of solids. [6] This shows that the method has significantly improved accuracy over the local or semi-local KS functionals which are, for example, currently used in the vast majority of heterogeneous catalysis calculations.

However, this is not satisfactory in many respects; for example the correct $-1/r$ dependence on the effective potential is not captured if the scaling is lower than 1. Therefore, in order to accurately describe Rydberg excited states, it is necessary to scale the correction by a factor of 1 to recover the correct $-1/r$ dependence, and PZ-SIC has been shown to describe such excited states accurately [9, 10, 13, 27]. Furthermore, in the context of a localized and delocalized structure dependent charge states of N,N'-dimethylpiperazine (DMP), which have been experimentally verified, it has been shown that when full SIC is applied to the PBE functional, an energy surface analogous to hybrid functionals with a Fock-Exchange weight of $\frac{1}{2}$ is obtained, while the scaling of SIC by $\frac{1}{2}$, only produces the more delocalized charge. [13]

KS–DFT depends only on the electron density and individual orbitals have no physical meaning. The energy is invariant under unitary rotations of occupied orbitals. PZ-SIC removes the SIE orbital-by-orbital and in a fully variational implementation, where the energy is minimized with respect to all electronic degrees of freedom ($dE/d\psi_k^* = 0$), the energy depends on individual orbitals which breaks the symmetry of the underlying theory and the SIC energy functional becomes unitary variant. Due

* hj@hi.is

† elvarorn@hi.is

to the full flexibility of fully variational SIC the lowest possible energy with respect to all degrees of freedom can be found, and even greater flexibility is achieved by using complex optimal orbitals. [25, 28] The unitary invariance of KS-DFT can be recovered in SIC energy functionals by restricting the degrees of freedom (and therefore narrow the search space), such as in the Fermi-Löwdin orbital SIC method, FLOSIC [29–31], where the electron density is decomposed into so-called Fermi-Orbitals (FOs), and instead the energy is minimized with respect to anchoring points in space which center the individual FOs.

In the present project, we further develop the fully variational SIC method and introduce a general local scaling function which bridges the gap in the application of fully variational SIC energy functionals to ground and excited states. In particular, this work lays important theoretical and numerical groundwork for improving the predictive accuracy of DFT in materials where accurate calculation are required for atomic or molecular properties, in combination with properties of solid substrates, such as in heterogeneous catalysis. We implement and evaluate a *locally scaled self-interaction correction* (LSSIC) scheme in the open source and python based GPAW code [32–34], where the LSSIC includes a spatial correction based on the degree of orbital localization, while taking into account that the orbitals are complex numbered. This approach retains the benefits of SIC in regions where it is most needed and accurately applied, such as for localised orbitals, while reducing or eliminating the correction in delocalised regions where error cancellations lead to an overcorrection.

II. THEORY

In Kohn-Sham density functional theory [1, 35] the energy of an electronic system is given by:

$$E^{\text{KS}} = T_s + V_{\text{ext}}[n] + E_C[n] + E_{xc}[n_{\uparrow}, n_{\downarrow}] \quad (1)$$

Here, T_s is the kinetic energy of the non-interacting electrons whose total density corresponds to the ground-state density of the interacting electrons. $V_{\text{ext}}[n]$ is the external potential describing attractive electron-nuclei Coulomb interaction. $E_C[n]$ is the repulsive electron-electron Coulomb interaction. Finally, $E_{xc}[n_{\uparrow}, n_{\downarrow}]$ is the exchange-correlation energy, a functional form which is not known exactly and is approximated in practice. For any semi-local functional – and for most hybrid functionals where fractional exact exchange is included – the electronic system possesses a spurious self-interaction error (SIE) due to the fact that there is only partial cancellation of the self Coulomb and exchange energies in the one-electron limit.

In PZ-SIC, the SIE is corrected orbital-by-orbital by removing the self Coulomb and self exchange-correlation energy resulting in

$$E^{\text{SIC}} = E^{\text{KS}}[n] - a \sum_{k\sigma} (E_C[n_{k\sigma}] + E_{xc}[n_{k\sigma}, 0]) \quad (2)$$

where a is a global scaling factor (i.e. $\frac{1}{2}$ or 1), and the sum is over all occupied orbitals k in spin channel σ . For the locally scaled SIC (LSSIC) the energy functional is further modified such that the orbital-by-orbital correction now includes a local function instead of the global scaling factor,

$$E^{\text{SIC}} = E^{\text{KS}}[n] - \sum_{k\sigma} (E_C[n_{k\sigma}, z_{\sigma}[\{n_{k\sigma}\}]] + E_{xc}[n_{k\sigma}, 0, z_{\sigma}[\{n_{k\sigma}\}]])) \quad (3)$$

where $z_{\sigma}[\{n_{k\sigma}\}] = z_{\sigma}(\mathbf{r})$. This is some local function of the occupied orbital spin densities.

We adopt an iso-orbital indicator as the scaling function – first introduced in the context of FLOSIC by Zope et. al. [31] – and apply it in this work to the fully variational SIC using complex optimal orbitals. In its most simple form it reads:

$$z_{\sigma}(\mathbf{r}) = \frac{\tau_{\sigma}^W(\mathbf{r})}{\tau_{\sigma}(\mathbf{r})} = \frac{\frac{|\nabla n_{\sigma}|^2}{8n_{\sigma}}}{\frac{1}{2} \sum_k |\nabla \psi_{k\sigma}|^2} \quad (4)$$

where the boundary conditions $0 \leq z_{\sigma}(\mathbf{r}) \leq 1$ are respected by construction, that is the local scaling function becomes zero in the limit of fully-delocalized states (i.e. the homogeneous electron gas limit) and is equal to one for single orbital densities (one electron systems) or orbital densities which are isolated – i.e. in regions where there is no overlap with other orbital densities (see Appendix B for derivation). Here τ_{σ} is the positive kinetic energy density for occupied orbitals with spin σ and $\tau_{\sigma}^W = \frac{|\nabla n_{\sigma}|^2}{8n_{\sigma}}$, is the von Weizsäcker kinetic energy density [36].

However, we re-derive the expressions for the von Weizsäcker kinetic energy density and Kohn-Sham kinetic energy density, taking into account that we have complex optimal orbitals, we arrive at the following generalized form of the iso-orbital indicator (see Appendix B):

$$z_{\sigma}(\mathbf{r}) = \frac{\frac{|\nabla n_{\sigma}(\mathbf{r})|^2}{8n_{\sigma}(\mathbf{r})} + \frac{1}{2} n_{\sigma}(\mathbf{r}) |\nabla \theta(\mathbf{r})|^2 - \frac{1}{4} \nabla^2 n_{\sigma}(\mathbf{r})}{\frac{1}{2} \sum_k f_{k\sigma} |\nabla \psi_{k\sigma}(\mathbf{r})|^2 - \frac{1}{4} \nabla^2 n_{\sigma}(\mathbf{r})} \quad (5)$$

where the second term in the nominator is the gradient of the phase term due to the use of complex numbered orbitals, and the third term in the nominator (and the second term in the denominator) is the Laplacian term. The Laplacian term arises for real and complex valued orbitals but is omitted in this work – and instead we write the local scaling function as

$$z_{\sigma}(\mathbf{r}) = \frac{\frac{|\nabla n_{\sigma}(\mathbf{r})|^2}{8n_{\sigma}(\mathbf{r})} + \frac{\mathbf{J}_{\sigma}(\mathbf{r}) \cdot \mathbf{J}_{\sigma}(\mathbf{r})}{2n_{\sigma}(\mathbf{r})}}{\frac{1}{2} \sum_k |\nabla \psi_{k\sigma}(\mathbf{r})|^2} \quad (6)$$

where the gradient of the complex phase term is written in terms of the current density $\mathbf{J}_{\sigma}(\mathbf{r}) =$

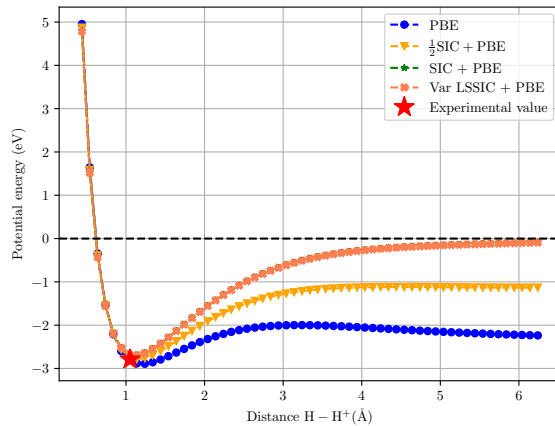


FIG. 1. Binding energy of H_2^+ calculated with $\frac{1}{2}\text{SIC}$ and SIC (yellow and green) and LSSIC (orange). The base functional is PBE (blue). The zero of energy corresponds to the dissociation limit $\text{H}+\text{H}^+$. Note that the SIC (green) and LSSIC (orange) curves perfectly overlap, since they are equivalent in the one-electron limit. The experimental estimate is marked on the plot (red star).

$-\frac{i}{2} \sum_k [\psi_{k\sigma}^*(\mathbf{r}) \nabla \psi_{k\sigma}(\mathbf{r}) - \psi_{k\sigma}(\mathbf{r}) \nabla \psi_{k\sigma}^*(\mathbf{r})]$, see [37, 38]. This iso-orbital scaling function is consistent with the derivation of both energy terms with complex optimal orbitals and has the same desirable property of $0 \leq z(\mathbf{r}) \leq 1$.

The orbital dependent SIE terms become

$$E_{\text{C}}[n_{i\sigma}, z_{\sigma}[n_{i\sigma}]] = \int \int \frac{z_{\sigma}(\mathbf{r}) n_{i\sigma}(\mathbf{r}) n_{i\sigma}(\mathbf{r}')}{|\mathbf{r} - \mathbf{r}'|} d\mathbf{r} d\mathbf{r}' \quad (7)$$

and

$$E_{\text{xc}}[n_{i\sigma}, 0, z_{\sigma}[n_{i\sigma}]] = \int z_{\sigma}(\mathbf{r}) n_{i\sigma}(\mathbf{r}) \epsilon_{\text{xc}}(\mathbf{r}) d\mathbf{r} \quad (8)$$

where $\epsilon_{\text{xc}}(\mathbf{r})$ is the exchange-correlation energy density. The functional derivative with respect to the occupied orbitals results in additional terms for the variational minimization of the total SIC energy functions, see Appendix A.

III. IMPLEMENTATION AND COMPUTATIONS

The locally scaled PZ-SIC energy functional is implemented in the open source grid-based projector augmented wave code GPAW [33, 34, 39]. The minimum (for ground state calculations) or saddle point (for excited state calculations) is found via a direct optimization method where the optimal orbitals are found variationally and self-consistently [26, 40, 41]. The unitary variant [42] of the projector augmented wave (PAW) method [43, 44] is used to treat the electrons near the nuclei (see

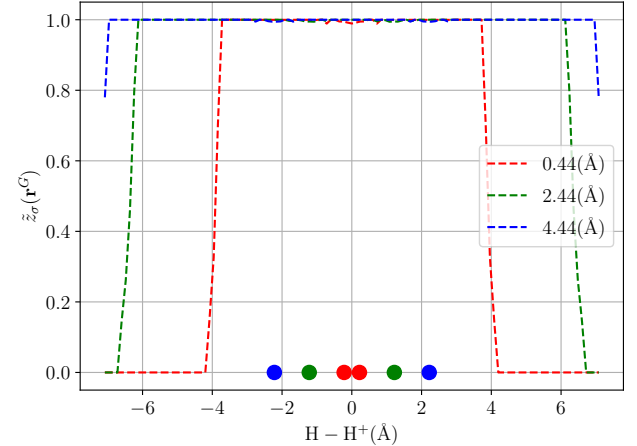


FIG. 2. Local scaling function evaluated with complex-valued pseudo-wavefunctions and pseudo-electron density of the H_2^+ molecule. The local scaling function is shown for different distances between the hydrogen and the hydrogen cation (indicated by the filled circles). In all cases the local scaling is approximately 1.0 in all space where the electron density is above a set threshold of $n_{\sigma}(\mathbf{r}) > 1e-12$ [au].

Appendix A). The core electrons for each atom are frozen to the result of a spherically symmetric calculation of the isolated atom. The smooth pseudo wave functions for the occupied MOs containing valence electrons are described here using a real-space grid, with a grid spacing of 0.16 Å. In the case of SIC calculation the wavefunctions are complex numbered.

In GPAW the “all-electron” electron spin density is given by

$$n_{\sigma}(\mathbf{r}) = \tilde{n}_{\sigma}(\mathbf{r}) + \sum_a (n_{\sigma}^a(\mathbf{r}) - \tilde{n}_{\sigma}^a(\mathbf{r})) + \frac{1}{2} n_c^a(\mathbf{r}) \quad (9)$$

where \tilde{n} is a smooth pseudo valence density which matches exactly with the smooth atomic partial density \tilde{n}^a within the PAW region. n^a is an “all-electron” atomic partial density. Finally, n_c^a are spherically symmetric atomic frozen core densities, where the factor $\frac{1}{2}$ accounts for the spin. We make use of the orthonormal property of the pseudo-valence states in UPAW and apply the locally scaled SIC energy functional to the pseudo density only. In this approximation the total pseudo-density is given by

$$\begin{aligned} \tilde{n}_{\sigma} &= \sum_k f_{k\sigma} \tilde{\psi}_{k\sigma}^* \tilde{\psi}_{k\sigma} + \frac{1}{2} \sum_a \tilde{\phi}_c^{a*} \tilde{\phi}_c^a \\ &= \sum_n f_{k\sigma} \tilde{\psi}_{k\sigma}^* \tilde{\psi}_{k\sigma} + \frac{1}{2} \sum_a \tilde{n}_c^a \end{aligned} \quad (10)$$

where the core electron density is given by smooth frozen core partial waves, $\tilde{\phi}_c^a$. The local scaling function in eq.

6 becomes

$$\tilde{z}_\sigma(\mathbf{r}) = \frac{\frac{|\nabla(\tilde{n}_\sigma(\mathbf{r}) + 1/2\tilde{n}_c(\mathbf{r}))|^2}{8(\tilde{n}_\sigma(\mathbf{r}) + 1/2\tilde{n}_c(\mathbf{r}))} + \frac{\tilde{\mathbf{J}}_\sigma(\mathbf{r}) \cdot \tilde{\mathbf{J}}_\sigma(\mathbf{r})}{2\tilde{n}_\sigma(\mathbf{r})}}{\frac{1}{2} \sum_i |\nabla \tilde{\psi}_{i\sigma}(\mathbf{r})|^2 + \frac{1}{4} \sum_{a\alpha} |\nabla \tilde{\phi}_\alpha^a(\mathbf{r})|^2}.$$

The total self-interaction corrected energy functional becomes

$$E^{\text{SIC}} = E^{\text{KS}}[n] - \sum_{i\sigma} (E_C[\tilde{n}_{k\sigma}, z_\sigma[\{\tilde{n}_{k\sigma}\}]] + E_{xc}[\tilde{n}_{k\sigma}, 0, z_\sigma[\{\tilde{n}_{k\sigma}\}]]). \quad (11)$$

A more detailed derivation of the local scaling function, resulting gradient and justification of the approximation given in eq. 11 is given in Appendix A and B. The gradient of the LSSIC energy functional is evaluated numerically using finite-difference, and represents the first realization of a fully variational locally scaled self-interaction corrected energy functional based on complex optimal orbitals.

In all cases the KS-DFT exchange-correlation functional is PBE [45] and we adopt the following nomenclature: PBE, $\frac{1}{2}$ SIC+PBE, SIC+PBE and LSSIC+PBE refer to calculations with the PBE energy functional, self interaction corrected PBE energy functional scaled by $\frac{1}{2}$ SIC and 1 and locally scaled self-interaction corrected PBE energy functional using eq. (6). In some cases we also present results for LSSIC with or without the complex phase term included, and "one shot" LSSIC, where we use an input pseudo-density and pseudo-wavefunctions from the PBE calculations to evaluate the local scaling function – and keep it fixed during the SCF calculation.

IV. APPLICATION

In the following section the fully variational LSSIC using complex optimal orbitals are applied to simple example systems and compared to GGA calculations, using the PBE energy functional, as well as and half- and SIC calculations (i.e. energy functional of eq. (2) with $a = 0.5$ and $a = 1.0$).

A. Hydrogen dimer cation

We start with the simplest possible molecule, namely the hydrogen dimer cation, H_2^+ , which has a single electron. It is well known that local and semi-local energy functionals predict the wrong dissociation limit where the electron is delocalized between the two hydrogens. The dimer binding potential energy surface is presented in Fig. 1 - and compared between the PBE energy functional, $\frac{1}{2}$ SIC, SIC, and LSSIC applied to the base functional. The hydrogen dimer cation is an important test system since it represents the simplest possible bond –

and contains a single electron. In this limit the PZ-SIC corrects exactly for the SIE – and does indeed give the correct dissociation limit. In Table I, the experimental bond energy and bond length of H_2^+ are compared to the PZ-SIC calculations. Although in terms of bond energy $\frac{1}{2}$ SIC yields the closest agreement to the experiment, it does not yield the correct dissociation limit since the binding energy is too low, because it only partially corrects for the SIE. SIC and variational LSSIC on the other hand do recover the correct dissociation limit, and at the same time provide a reasonable estimate for the bond energy and bond length of H_2^+ . Unsurprisingly, these two calculations match exactly, since the localscaling function effectively scales the SIC by a factor of 1.0 in all space in the one-electron limit. H_2^+ described with the PBE energy functional dissociates into two partially charged hydrogen atoms, which yields an unphysical dissociation limit. Fig. 2 shows the binding energy of H_2^+ and the dissociation limits of the PBE and SIC calculations.

B. Electron affinity and ionization energy of atoms

Table II lists the electron affinity (EA) and ionization energy (IE) of the Carbon(C), Nitrogen(N) and Oxygen(O) atoms, and Fig. 3 presents bar plots showing the deviation of the calculated values from experiment for the O atom. Results are presented for the PBE energy functional, $\frac{1}{2}$ SIC, SIC and variational and one shot LSSIC - and compared to experimental results (extracted from the NIST database). In all cases the PBE functional gives an EA which is too low – i.e. the additional electron is bound too strongly, and an IE which is too high – i.e. it holds on the highest occupied valence electron too tightly. $\frac{1}{2}$ SIC improves the estimate for the EA significantly, as well as for the IE, and gives the overall best result compared to experiment. SIC tends to overcorrect the SIE in the case of EA, and now instead the EA is too high compared to experiment – i.e. the extra electron is bound to weakly. For the IE, SIC gives the best agreement with experiment, and deviates less than 1% from experiment. Variational LSSIC predicts EAs for N and O in close agreement with experiments. The differences are 0.104eV and 0.065eV to the experimental results respectively. In fact, the variational LSSIC calculations are closest to the experimental values compared to the other energy functionals. However, they underestimate the correction to the SIE in the case of the C EA. Variational LSSIC only slightly improves the IE for C and N compared to the PBE functional. Note that the effect of the inclusion of the complex phase term in the local scaling function marginally improves the prediction of the IE for N and O, as well as the EA, but is negligible in the EA and IE for C. One shot LSSIC performs the worst in comparison with the other SIE corrected energy functionals. It tends to over-correct the SIE when calculating the EA, and yields similar results when compared to SIC, whereas it completely under-corrects the SIE when cal-

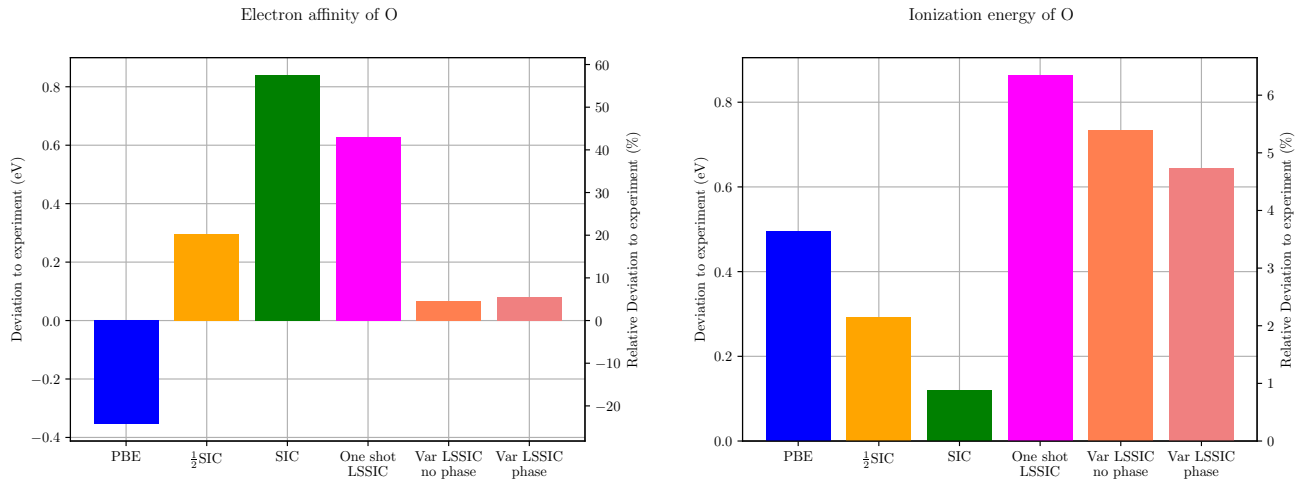


FIG. 3. Left: bar plot showing the deviation of the calculated electron affinity from the experimental result. Right: bar plot showing the deviation of the calculated ionization energy from the experimental result. In both plots, the numerical values in electron-volts are given on the left y-axis, and the relative deviation is given on the right y-axis.

culating the IE, where it yields similar results as the base functional PBE for C and N.

All in all the variational LSSIC, including the gradient of the complex phase, gives the best agreement with experiment for the electron affinity of these atoms. For the ionization energies, it either only marginally improves the results, or in the case of O does not improve compared to the PBE functional. However, there is a very clear improvement in the IE of O when using the LSSIC with the gradient of the complex phase compared to the one-shot LSSIC and LSSIC without the gradient of the complex phase, this can be seen in Fig. 3.

C. Dimers

Here the potential energy surface of the carbon, nitrogen and oxygen dimers are calculated using PBE, $\frac{1}{2}$ SIC, SIC and the three flavors of LSSIC - with and without the gradient of the phase term included, and one-shot LSSIC, where the input density is from a converged PBE calculation (and therefore has no phase since the converged PBE wavefunctions have no phase). Fig. 4 presents the local scaling function for the carbon dimer evaluated along the bond axis and at two distances – close to the experimental bond length, where the spin densities are spatially symmetric, and at a large separation where it is clear that one spin channel is localized preferentially on one of the carbon atoms (and vice versa).

Table I presents the bond energy and bond lengths as predicted by all of the energy functionals and provides the corresponding experimental results. For C, N and O, PBE overestimates the bond energy – with almost a 1 eV overestimation for the oxygen dimer bond energy – but at the same time has the overall best agreement with the bond length compared to experiment. SIC on

TABLE I. Equilibrium bond lengths and bond energies for C_2 , N_2 , O_2 and H_2^+ . Results are shown for the PBE, $\frac{1}{2}$ SIC and SIC energy functionals, as well as LSSIC with (phase) and without (no phase) the gradient of the complex phase included in the local scaling function. One shot LSSIC is also presented where the local scaling function is calculated once with the converged PBE electron spin density. Experimental results were obtained from [46, 47].

Dimer	Calculation	Energy (eV)	Bond length (\AA)
C_2	PBE	-6.503	1.235
	$\frac{1}{2}$ SIC	-6.140	1.217
	SIC	-5.879	1.206
	Var LSSIC no phase	-6.466	1.211
	Var LSSIC phase	-6.471	1.212
	Oneshot LSSIC no phase	-6.380	1.210
N_2	Experiment	-6.355	1.242
	PBE	-10.514	1.104
	$\frac{1}{2}$ SIC	-10.096	1.091
	SIC	-9.732	1.081
	Var LSSIC no phase	-10.381	1.091
	Var LSSIC phase	-10.382	1.091
O_2	Oneshot LSSIC no phase	-10.380	1.092
	Experiment	-9.924	1.098
	PBE	-6.235	1.219
	$\frac{1}{2}$ SIC	-5.479	1.188
	SIC	-4.840	1.166
	Var LSSIC no phase	-5.400	1.190
H_2^+	Var LSSIC phase	-5.413	1.189
	Oneshot LSSIC no phase	-5.201	1.190
	Experiment	-5.213	1.207
	PBE	-2.893	1.208
	$\frac{1}{2}$ SIC	-2.782	1.154
	SIC	-2.694	1.117
Var LSSIC	Var LSSIC	-2.694	1.117
	Experiment	-2.790	1.052

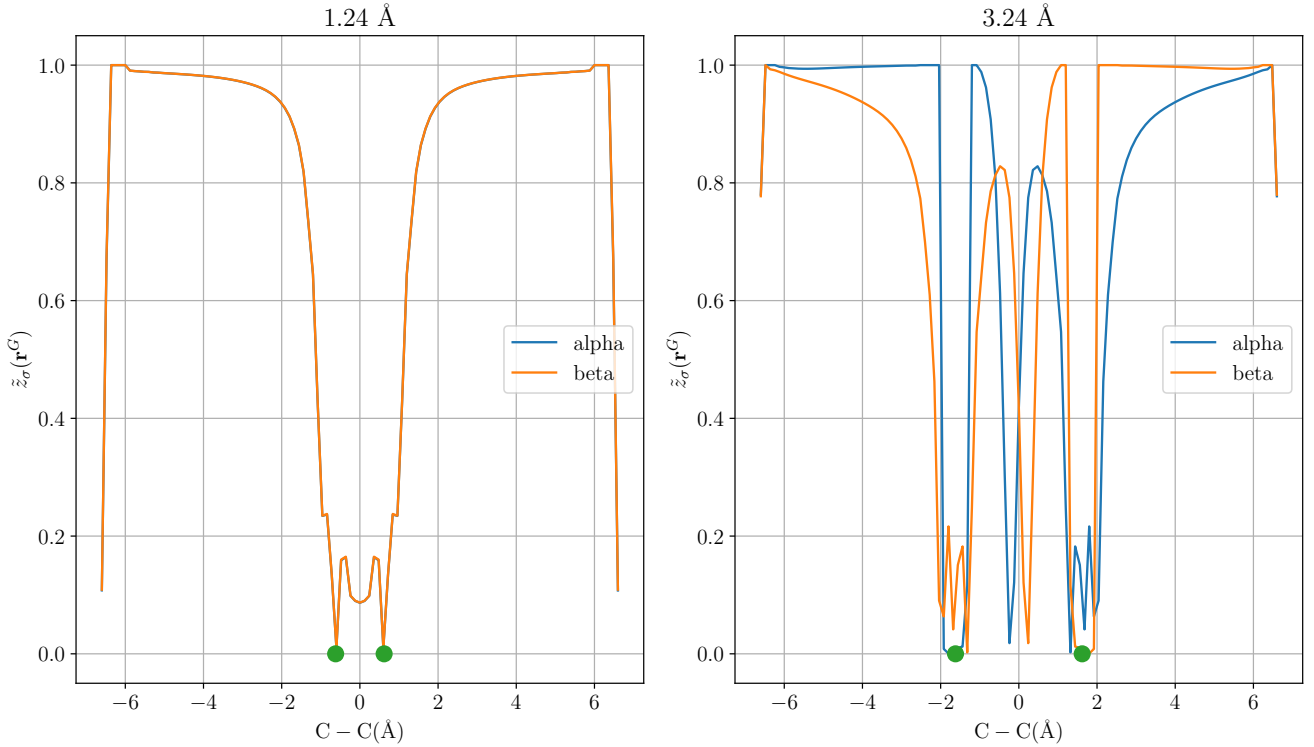


FIG. 4. Localscaling function evaluated for the carbon dimer at two distances - 1.24 Å, which is close to the experimental bond length, and 3.24 Å. Both spin channels are presented and are denoted alpha (blue) and beta (orange). It is clear that the spin densities are symmetric in all space when the distance is close to the experimental bond length, whereas the spin densities are spatially different as we approach the dissociation limit, with one spin being preferentially concentrated on one carbon vs the other. The green dots denote the position of the carbon nuclei along the axis which is parallel to the bond.

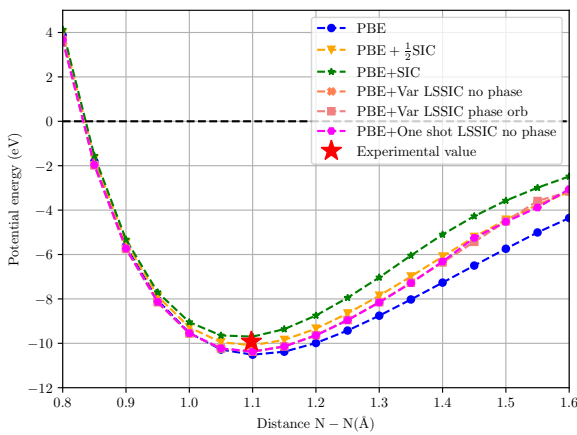


FIG. 5. Potential energy of the nitrogen dimer as a function of distance. The experimental estimate is marked on the plot (red star).

the other hand over corrects the SIE and predicts in all cases a bond energy which is too low, and a bond length which is too short.

$\frac{1}{2}$ SIC presents a good compromise in all cases, since it on average yields the best agreement to experimental values in terms of both bond energy and bond length. LSSIC with and without the gradient of the complex phase results in closer agreement to the experimental values in terms of the bond energy for both C and O compared to the PBE, $\frac{1}{2}$ SIC and SIC. One shot LSSIC gives a remarkably good agreement for the bond energy of both C and O dimers. The bond energy calculated by One shot LSSIC differs 0.025eV and 0.012eV from the experiment respectively.

The greatest deviation for LSSIC in terms of the bond energy is for the N dimer, and the various different potential energy surfaces are shown in Fig. 5. LSSIC only slightly improves the bond energy compared to PBE in this case. While LSSIC predicts a too large bond energy, compared to experiment and $\frac{1}{2}$ SIC, the general curve after the equilibrium bond length tends to follow the $\frac{1}{2}$ SIC curve.

V. CONCLUSION & OUTLOOK

We have presented a fully variational locally scaled self-interaction corrected energy functional, using com-

TABLE II. Electron affinity (EA) and ionization energy (IE) for C, N, and O (eV). Results are shown for the PBE, $\frac{1}{2}$ SIC and SIC energy functionals, as well as LSSIC with (phase) and without (no phase) the gradient of the complex phase included in the local scaling function. One shot LSSIC is also presented where the local scaling function is calculated once with the converged PBE electron spin density. Experimental results were obtained from [48].

Element	Functional	EA (eV)	IE (eV)
C	PBE	-1.606	11.622
	$\frac{1}{2}$ SIC	-1.290	11.450
	SIC	-1.037	11.273
	Var LSSIC no phase	-1.534	11.564
N	Var LSSIC phase	-1.535	11.563
	One shot SIC	-1.007	11.505
	Experiment	-1.261	11.26
	PBE	-0.331	14.917
O	$\frac{1}{2}$ SIC	0.251	14.773
	SIC	0.684	14.637
	Var LSSIC no phase	-0.041	14.923
	Var LSSIC phase	-0.033	14.858
	One shot SIC	0.427	14.739
	Experiment	0.071	14.53
	PBE	-1.813	14.104
	$\frac{1}{2}$ SIC	-1.165	13.902
	SIC	-0.620	13.729
	Var LSSIC no phase	-1.395	14.343
	Var LSSIC phase	-1.381	14.254
	One shot SIC	-0.833	14.472
	Experiment	-1.460	13.61

plex optimal orbitals. The new energy functional cap-

tures the exact PES of the hydrogen cation - since in the limit of a single electron the SIC energy is captured (and is formally an exact correction). In the case of the C, N and O atoms the locally scaled SIC improves the prediction of electron affinity, whereas it does not improve the prediction of ionization energies, compared to the PBE functional. For the multi-electron dimers considered in this work, all LSSIC energy functionals predict a reasonable bond energy and equilibrium bond distance, i.e. within 4% and 3% of the experimental value respectively. This shows that the local scaling SIC energy functional is either on a similar footing as other energy functional methods, or improve the predicted properties. The local scaling SIC is a general framework, in the sense that the local scaling function can be tweaked and tuned by introducing scaling parameters and or other functions based on the electron density. In future work the shape of the local scaling function will be optimized in order to best capture the properties of atoms and molecules, as well as defect states in solid-systems.

ACKNOWLEDGMENTS

We thank Prof. Gianluca Levi and Dr. Aleksei Ivanov for fruitful discussions and insights. This work was supported by the Innovation Fund, grant agreement no. 2513106, and the Icelandic Research Fund, grant agreement no. 2410644. Computer resources, data storage, and IT user support were provided by the Icelandic Research e-Infrastructure (IREI), funded by the Icelandic Infrastructure Fund.

[1] W. Kohn and L. J. Sham, Self-consistent equations including exchange and correlation effects, *Phys. Rev.* **140**, A1133 (1965).

[2] W. Kohn, Nobel lecture: Electronic structure of matter—wave functions and density functionals, *Rev. Mod. Phys.* **71**, 1253 (1999).

[3] J. Lægsgaard and K. Stokbro, Hole trapping at al impurities in silica: A challenge for density functional theories, *Phys. Rev. Lett.* **86**, 2834 (2001).

[4] M. Nolan and G. W. Watson, The electronic structure of alkali doped alkaline earth metal oxides: Li doping of mgo studied with dft-gga and gga+u, *Surface Science* **586**, 25 (2005).

[5] G. Pacchioni, Electronic interactions and charge transfers of metal atoms and clusters on oxide surfaces, *Phys. Chem. Chem. Phys.* **15**, 1737 (2013).

[6] H. Gudmundsdóttir, E. Jonsson, and H. Jonsson, Calculations of al dopant in alpha-quartz using a variational implementation of the perdew–zunger self-interaction correction, *New Journal of Physics* **17**, 083006 (2015).

[7] A. V. Ivanov, Y. L. A. Schmerwitz, G. Levi, and H. Jonsson, Electronic excitations of the charged nitrogen-vacancy center in diamond obtained using time-independent variational density functional calculations, *SciPost Phys.* **15**, 009 (2023).

[8] M. Galynska, J. E. Örn, and H. Jonsson, Ground and excited state of li doped mgo described with perdew-zunger self-interaction correction, (in preparation) (2025).

[9] H. Gudmundsdóttir, Y. Zhang, P. M. Weber, and H. Jonsson, Self-interaction corrected density functional calculations of molecular rydberg states, *The Journal of Chemical Physics* **139**, 194102 (2013).

[10] H. Gudmundsdóttir, Y. Zhang, P. M. Weber, and H. Jonsson, Self-interaction corrected density functional calculations of rydberg states of molecular clusters: N,n-dimethylisopropylamine, *The Journal of Chemical Physics* **141**, 234308 (2014).

[11] A. E. Sigurdarson, Y. L. A. Schmerwitz, D. K. V. Tveiten, G. Levi, and H. Jonsson, Orbital-optimized density functional calculations of molecular rydberg excited states with real space grid representation and self-interaction correction, *The Journal of Chemical Physics* **159**, 214109 (2023).

[12] E. Selenius, A. E. Sigurdarson, Y. L. A. Schmerwitz, and G. Levi, Orbital-optimized versus time-dependent density functional calculations of intramolecular charge transfer excited states, *Journal of Chemical Theory and Computation* **20**, 3809 (2024).

[13] B. O. Birgisson, M. Gałyńska, H. Myneni, E. Ö. Jónsson, R. Björnsson, and H. Jonsson, Localized and delocalized charge distribution in a diamine cation and rydberg excited state: A challenging test for density functionals, *The Journal of Physical Chemistry Letters* **16**, 5844 (2025).

[14] A. V. Ivanov, T. K. Ghosh, E. Jonsson, and H. Jónsson, Mn dimer can be described accurately with density functional calculations when self-interaction correction is applied, *The Journal of Physical Chemistry Letters* **12**, 4240–4246 (2021).

[15] R. Maniar, P. B. Shukla, J. K. Johnson, K. A. Jackson, and J. P. Perdew, Atomic ionization: sd energy imbalance and perdew–zunger self-interaction correction energy penalty in 3d atoms, *Proceedings of the National Academy of Sciences* **122**, e2418305122 (2025).

[16] S. Klüpfel, P. Klüpfel, and H. Jonsson, The effect of the perdew–zunger self-interaction correction to density functionals on the energetics of small molecules, *The Journal of Chemical Physics* **137**, 10.1063/1.4752229 (2012).

[17] R. Urrego-Ortiz, S. Builes, F. Illas, and F. Calle-Vallejo, Gas-phase errors in computational electrocatalysis: A review, *EES Catalysis* **2**, 157–179 (2024).

[18] J. P. Perdew and A. Zunger, Self-interaction correction to density-functional approximations for many-electron systems, *Phys. Rev. B* **23**, 5048 (1981).

[19] E. Bylaska, K. Tsemekhman, and H. Jonsson, Self-consistent self-interaction corrected DFT: The method and applications to extended and confined systems, *APS* **2004**, L38 (2004).

[20] H. Jónsson, Simulation of surface processes, *Proceedings of the National Academy of Sciences* **108**, 944 (2011), <http://www.pnas.org/content/108/3/944.full.pdf>.

[21] I. Dabo, A. Ferretti, N. Poilvert, Y. Li, N. Marzari, and M. Cococcioni, Koopmans condition for density-functional theory, *Phys. Rev. B* **82**, 115121 (2010).

[22] O. A. Vydrov, G. E. Scuseria, J. P. Perdew, A. Ruzsinszky, and G. I. Csonka, Scaling down the perdew–zunger self-interaction correction in many-electron regions, *Journ. Chem. Phys.* **124**, 094108 (2006), <https://doi.org/10.1063/1.2176608>.

[23] S. Klüpfel, P. Klüpfel, and H. Jónsson, The effect of the perdew–zunger self-interaction correction to density functionals on the energetics of small molecules, *J. Chem. Phys.* **137**, 124102 (2012), <https://doi.org/10.1063/1.4752229>.

[24] E. O. Jonsson, S. Lehtola, and H. Jonsson, Towards an optimal gradient-dependent energy functional of the pzsic form, *Procedia Computer Science* **51**, 1858–1864 (2015).

[25] S. Lehtola, E. Jonsson, and H. Jonsson, Effect of complex-valued optimal orbitals on atomization energies with the perdew–zunger self-interaction correction to density functional theory, *Journal of Chemical Theory and Computation* **12**, 4296–4302 (2016).

[26] Y. L. Schmerwitz, A. V. Ivanov, E. Jonsson, H. Jonsson, and G. Levi, Variational density functional calculations of excited states: Conical intersection and avoided crossing in ethylene bond twisting, *The Journal of Physical Chemistry Letters* **13**, 3990–3999 (2022).

[27] X. Cheng, Y. Zhang, S. Deb, M. P. Miniti, Y. Gao, H. Jonsson, and P. M. Weber, Ultrafast structural dynamics in rydberg excited n,n,n,n-tetramethylethylenediamine: conformation dependent electron lone pair interaction and charge delocalization, *Chem. Sci.* **5**, 4394 (2014).

[28] S. Lehtola and H. Jónsson, Variational, self-consistent implementation of the perdew–zunger self-interaction correction with complex optimal orbitals, *J. Chem. Theo. Comput.* **10**, 5324 (2014).

[29] K. A. Jackson, J. E. Peralta, R. P. Joshi, K. P. Withanage, K. Trepte, K. Sharkas, and A. I. Johnson, Towards efficient density functional theory calculations without self-interaction: The fermi–löwdin orbital self-interaction correction, arXiv preprint [arXiv:1910.10677](https://arxiv.org/abs/1910.10677), 10.48550/ARXIV.1910.10677 (2019), [arXiv:1910.10677](https://arxiv.org/abs/1910.10677) [physics.chem-ph].

[30] M. R. Pederson, Fermi orbital derivatives in self-interaction corrected density functional theory: Applications to closed shell atoms, arXiv preprint [arXiv:1412.3101](https://arxiv.org/abs/1412.3101), 10.48550/arXiv.1412.3101 (2014), [arXiv:1412.3101](https://arxiv.org/abs/1412.3101) [physics.chem-ph].

[31] R. R. Zope, Y. Yamamoto, C. M. Diaz, T. Baruah, J. E. Peralta, K. A. Jackson, B. Santra, and J. P. Perdew, A step in the direction of resolving the paradox of perdew–zunger self-interaction correction, *The Journal of Chemical Physics* **151**, 214108 (2019).

[32] J. J. Mortensen, A. H. Larsen, M. Kuisma, A. V. Ivanov, A. Taghizadeh, A. Peterson, A. Haldar, A. O. Dohn, C. Schafer, E. Ö. Jónsson, E. D. Hermes, F. A. Nilsson, G. Kastlunger, G. Levi, H. Jonsson, H. Häkkinen, J. Fojt, J. Kangasbanik, J. Sødequist, J. Lehtomäki, J. Heske, J. Enkovaara, K. T. Winther, M. Dulak, M. M. Melander, M. Ovesen, M. Louhivuori, M. Walter, M. Gjerding, O. Lopez-Acevedo, P. Erhart, R. Warmbier, R. Würdemann, S. Kaappa, S. Latini, T. M. Boland, T. Bligaard, T. Skovhus, T. Susi, T. Maxson, T. Rossi, X. Chen, Y. L. A. Schmerwitz, J. Schiøtz, T. Olsen, K. W. Jacobsen, and K. S. Thygesen, Gpaw: Open python package for electronic-structure calculations, *The Journal of Chemical Physics* (in press) **160**, 10.1063/5.0182685 (2024).

[33] J. Enkovaara, C. Rostgaard, J. J. Mortensen, J. Chen, M. Dulak, L. Ferrighi, J. Gavnholt, C. Glinsvad, V. Haikola, H. A. Hansen, H. H. Kristoffersen, M. Kuisma, A. H. Larsen, L. Lehtovaara, M. Ljungberg, O. Lopez-Acevedo, P. G. Moses, J. Ojanen, T. Olsen, V. Petzold, N. A. Romero, J. Stausholm-Møller, M. Strange, G. A. Tritsaris, M. Vanin, M. Walter, B. Hammer, H. Häkkinen, G. K. H. Madsen, R. M. Nieminen, J. K. Nørskov, M. Puska, T. T. Rantala, J. Schiøtz, K. S. Thygesen, and K. W. Jacobsen, Electronic structure calculations with gpaw: a real-space implementation of the projector augmented-wave method, *J. Phys. Condens. Matter* **22**, 253202 (2010).

[34] J. J. Mortensen, A. H. Larsen, M. Kuisma, A. V. Ivanov, A. Taghizadeh, A. Peterson, A. Haldar, A. O. Dohn, C. Schäfer, E. Ö. Jónsson, E. D. Hermes, F. A. Nilsson, G. Kastlunger, G. Levi, H. Jónsson, H. Häkkinen, J. Fojt, J. Kangasbanik, J. Sødequist, J. Lehtomäki, J. Heske, J. Enkovaara, K. T. Winther, M. Dulak, M. M. Melander, M. Ovesen, M. Louhivuori, M. Walter, M. Gjerding, O. Lopez-Acevedo, P. Erhart, R. Warmbier, R. Würdemann, S. Kaappa, S. Latini, T. M. Boland, T. Bligaard, T. Skovhus, T. Susi, T. Maxson, T. Rossi, X. Chen, Y. L. A. Schmerwitz, J. Schiøtz, T. Olsen, K. W. Jacobsen, and K. S. Thygesen, Gpaw: An open python package for electronic structure calculations, *J. Chem. Phys.* **160**, 092503 (2024).

- [35] P. Hohenberg and W. Kohn, Inhomogeneous electron gas, *Phys. Rev.* **136**, B864 (1964).
- [36] R. Parr and W. Yang, *Density-Functional Theory of Atoms and Molecules* (Oxford University Press, Oxford, 1989).
- [37] A. D. Becke, Current-density dependent exchange-correlation functionals, *Canadian journal of chemistry* **74**, 995 (1996).
- [38] E. R. Johnson, R. M. Dickson, and A. D. Becke, Density functionals and transition-metal atoms, *The Journal of chemical physics* **126**, 10.1063/1.2723118 (2007).
- [39] J. Mortensen, L. Hansen, and K. W. Jacobsen, Real-space grid implementation of the projector augmented wave method, *Phys. Rev. B* **71**, 035109 (2005).
- [40] A. V. Ivanov, E. Jonsson, T. Vegge, and H. Jonsson, Direct energy minimization based on exponential transformation in density functional calculations of finite and extended systems, *Computer Physics Communications* **267**, 108047 (2021).
- [41] A. V. Ivanov, G. Levi, E. Ö. Jonsson, and H. Jonsson, Method for calculating excited electronic states using density functionals and direct orbital optimization with real space grid or plane-wave basis set, *Journal of Chemical Theory and Computation* **17**, 5034 (2021).
- [42] A. V. Ivanov, A. Patterson, M. Bothe, C. Sünderhauf, B. K. Berntson, J. J. Mortensen, M. Kuisma, E. Campbell, and R. Izsák, *Quantum computation of electronic structure with projector augmented-wave method and plane wave basis set* (2024), arXiv:2408.03159 [quant-ph].
- [43] P. E. Blöchl, Projector augmented-wave method, *Phys. Rev. B* **50**, 17953 (1994).
- [44] P. E. Blöchl, C. J. Först, and J. Schimpl, Projector augmented wave method:ab initio molecular dynamics with full wave functions, *Bull. Mater. Sci.* **26**, 33 (2003).
- [45] J. P. Perdew, K. Burke, and M. Ernzerhof, Generalized gradient approximation made simple, *Phys. Rev. Lett.* **77**, 3865 (1996).
- [46] B. deB. Darwent, *Bond Dissociation Energies in Simple Molecules*, Tech. Rep. 31 (National Bureau of Standards (U.S.), Washington, D.C., 1970) issued January 1970.
- [47] National Institute of Standards and Technology, *NIST Chemistry WebBook, Standard Reference Database 69*, Tech. Rep. (National Institute of Standards and Technology, 2025) accessed January 2026; chemical property data for compounds including H₂⁺, O₂, C₂, and N₂.
- [48] Wolfram Research, *ElementData, wolfram language function* (2014), accessed Jan 2026.
- [49] Z. Romanowski and S. Krukowski, Derivation of von weizsäcker equation based on green–gauss theorem, *Acta Physica Polonica A* **115**, 653 (2009).

Appendix A: Implementation in GPAW

Within the PAW formalism, the so-called “all-electron” wave functions, which contain cusps at the positions of the nuclei, are written as

$$\psi_{i,\sigma}(\mathbf{r}) = \hat{\mathcal{T}}\tilde{\psi}_{i,\sigma}(\mathbf{r}) \quad (\text{A1})$$

where $\tilde{\psi}_{i,\sigma}$ are “pseudo-electron” wave functions, which are smooth everywhere. $\hat{\mathcal{T}}$ is a linear transformation operator, which corrects for the smooth description of the

electronic wave functions near the positions of the nuclei

$$\hat{\mathcal{T}} = 1 + \sum_{a\alpha} (|\varphi_{\alpha}^a\rangle - |\tilde{\varphi}_{\alpha}^a\rangle) \langle \tilde{p}_{\alpha}^a | \quad (\text{A2})$$

Here, φ_{α}^a and $\tilde{\varphi}_{\alpha}^a$ are partial waves describing the all-electron and pseudo-electron wave functions in an atomic region of radius r_c^a around each nucleus a . The all-electron and pseudo-electron partial waves are required to be identical beyond the radius r_c^a , i.e. $\varphi_{\alpha}^a(\mathbf{r}) = \tilde{\varphi}_{\alpha}^a(\mathbf{r})$ for $|\mathbf{r} - \mathbf{R}^a| > r_c^a$. \tilde{p}_{α}^a are smooth projection functions, which satisfy

$$\sum_{\alpha} |\tilde{\varphi}_{\alpha}^a\rangle \langle \tilde{p}_{\alpha}^a| = 1 \quad \text{for } |\mathbf{r} - \mathbf{R}^a| \leq r_c^a \quad (\text{A3})$$

$$\langle \tilde{p}_{\alpha}^a | \tilde{\varphi}_{\beta}^a \rangle = \delta_{\alpha\beta} \quad \text{for } |\mathbf{r} - \mathbf{R}^a| \leq r_c^a \quad (\text{A4})$$

such that

$$|\tilde{\psi}_{i,\sigma}\rangle = \sum_{\alpha} |\tilde{\varphi}_{\alpha}^a\rangle P_{\alpha i,\sigma}^a \quad \text{for } |\mathbf{r} - \mathbf{R}^a| \leq r_c^a \quad (\text{A5})$$

$$|\psi_{i,\sigma}\rangle = \sum_{\alpha} |\varphi_{\alpha}^a\rangle P_{\alpha i,\sigma}^a \quad \text{for } |\mathbf{r} - \mathbf{R}^a| \leq r_c^a \quad (\text{A6})$$

where $P_{\alpha i,\sigma}^a = \langle \tilde{p}_{\alpha}^a | \tilde{\psi}_{i,\sigma} \rangle$, i.e. the all- and pseudo-electron wave functions can be expanded into partial waves with the same linear expansion coefficients.

We use unitary projector augmented wave (UPAW), which has recently been implemented in GPAW [42] to describe the frozen core electrons and pseudo- to all-electron transformation. In UPAW the transformation operator is enforced to fulfill:

$$\hat{O} = \hat{\tau}^\dagger \hat{\tau} = I \quad (\text{A7})$$

i.e. $\hat{\tau}^\dagger = \hat{\tau}^{-1}$. This is realized by enforcing the partial wave projector operator to satisfy:

$$\Delta \hat{O} = \sum_a \sum_{ij} |\tilde{p}_i^a\rangle \langle \tilde{p}_j^a| = 0 \quad (\text{A8})$$

which is guaranteed if

$$O_{ij}^a = \langle \phi_i^a | \phi_j^a \rangle - \langle \tilde{\phi}_i^a | \tilde{\phi}_j^a \rangle = 0 \quad (\text{A9})$$

Hence, in order to construct a UPAW augmentation region the overlap of the ij pair of pseudo partial waves and the ij pair of all-electron partial waves must be the same. A direct consequence of UPAW is that the pseudo-valence states naturally become orthonormal

$$\int_V \tilde{\psi}_n^*(\mathbf{r}) \tilde{\psi}_m(\mathbf{r}) d\mathbf{r} = \delta_{nm} \quad (\text{A10})$$

and the pseudo-valence density integrates to the stoichiometric number of valence electrons (in charge neutral systems), or

$$\int_V \tilde{n}(\mathbf{r}) d\mathbf{r} = \int_V n(\mathbf{r}) d\mathbf{r} = n_{\text{valence}} \quad (\text{A11})$$

The Hamiltonian fully separates into a pseudo and atomic PAW correction, and the pseudo part can be trivially solved

$$(\tilde{H}(\mathbf{r}) - \epsilon_n) \tilde{\psi}_n(\mathbf{r}) = 0 \quad (\text{A12})$$

i.e. the pseudo-valence states are eigenvectors of the pseudo-Hamiltonian. Atomic corrections can be selectively included in the Hamiltonian without loss of generality, due to the linear mapping between the atomic and grid region.

Therefore we write an approximate, but variationally self-consistent, SIC term with scaling as

$$\begin{aligned} E^{\text{SIC}} &= E^{\text{KS}}[n] \\ &- \frac{1}{2} \sum_{i\sigma} (E_C[\tilde{n}_{i\sigma}, z[\tilde{n}_{i\sigma}]] + E_{xc}[\tilde{n}_{i\sigma}, z[\tilde{n}_{i\sigma}], 0]) \end{aligned} \quad (\text{A13})$$

i.e. we do not calculate the SIC part of the PAW correction associated with the UPAW.

The energy functional and resulting Hamiltonian is orbital density dependent and therefore requires an optimization method which finds the optimal orbitals that minimizes the total SIC energy functional

$$\min_{\psi_i} E^{\text{SIC}}[\{\psi_i\}]$$

To that end the minimum of the functional is found via a direct optimization method where the optimal orbitals are found variationally and self-consistently [26, 40, 41]. These orbitals must satisfy the Euler-Lagrange equations (the spin index σ is omitted for clarity):

$$f_i (\hat{h} + \hat{v}_i) |\psi_i\rangle = \sum_j |\psi_j\rangle \lambda_{ji} \quad (\text{A14})$$

$$\hat{h} = -\frac{1}{2} \Delta + v_{ext} + v_C[n] + v_{xc}[n] \quad (\text{A15})$$

$$\hat{v}_i = -\frac{1}{2} (v_C[\tilde{n}_i, z[\tilde{n}_i]] + v_{xc}[\tilde{n}_i, z[\tilde{n}_i]]) \quad (\text{A16})$$

where f_i is the occupation number of the i^{th} orbital $|\psi_i\rangle$, λ_{ji} is a Lagrange multiplier which enforces orthogonality between orbital pairs ij . v_{ext} is the external potential, v_H and v_{xc} are Hartree and the exchange-correlation potentials, respectively, n is the total density, and n_i is the i^{th} orbital density.

Due to the local scaling function additional terms are needed (other than the orbital dependent Coulomb and exchange-correlation potential) in the orbital dependent potential operator \hat{v}_i . These are

$$\begin{aligned} v_C[\tilde{n}_i, z[\tilde{n}_i]] &= \sum_j \frac{\partial E_C[\tilde{n}_i, z[\tilde{n}_i]]}{\partial \tilde{n}_j(\mathbf{r}'')} \\ &= \frac{1}{2} \sum_j \frac{\partial}{\partial \tilde{n}_j(\mathbf{r}'')} \iint \frac{z(\mathbf{r}) \tilde{n}_i(\mathbf{r}) \tilde{n}_i(\mathbf{r}')}{|\mathbf{r} - \mathbf{r}'|} d\mathbf{r} d\mathbf{r}' \\ &= \frac{1}{2} z(\mathbf{r}'') \int \frac{\tilde{n}_i(\mathbf{r}')}{|\mathbf{r}' - \mathbf{r}''|} d\mathbf{r}' + \frac{1}{2} \int \frac{z(\mathbf{r}) \tilde{n}_i(\mathbf{r})}{|\mathbf{r} - \mathbf{r}''|} d\mathbf{r} \\ &\quad + \frac{1}{2} \sum_j \frac{\partial z(\mathbf{r}'')}{\partial \tilde{n}_i(\mathbf{r}'')} \tilde{n}_j(\mathbf{r}'') \int \frac{\tilde{n}_j(\mathbf{r}')}{|\mathbf{r}'' - \mathbf{r}'|} d\mathbf{r}' \end{aligned} \quad (\text{A17})$$

and

$$\begin{aligned} v_{xc}[\tilde{n}_i, z[\tilde{n}_i]] &= \sum_j \frac{\partial E_{xc}[\tilde{n}_i, 0, z[\tilde{n}_i]]}{\partial \tilde{n}_j(\mathbf{r}'')} \\ &= \sum_j \frac{\partial}{\partial \tilde{n}_j(\mathbf{r}'')} \int z(\mathbf{r}) \tilde{n}_i(\mathbf{r}) \epsilon_{xc}(\tilde{n}_i, 0) d\mathbf{r} \\ &= z(\mathbf{r}'') \tilde{v}_{xc,i}(\mathbf{r}'') \\ &\quad + \sum_j \frac{\partial z(\mathbf{r}'')}{\partial \tilde{n}_i(\mathbf{r}'')} \tilde{n}_j(\mathbf{r}'') \epsilon_{xc}(\tilde{n}_j, 0) \end{aligned} \quad (\text{A18})$$

Appendix B: Derivation of the local scaling function

The following provides a concise derivation of the kinetic energy densities entering the iso-orbital indicator used as a local scaling function in PZ-SIC. The derivation closely follows that of Romanowski and Krukowski [49], but is written here allowing for complex-valued orbitals. The resulting expressions define the kinetic energy densities used in this work, which are subsequently combined to form the local scaling function.

Generalised von Weizsäcker Kinetic Energy Density

We start with the standard definition of kinetic energy T for a single wavefunction $\psi(\mathbf{r})$:

$$T = -\frac{1}{2} \int_{\mathbb{R}^3} \psi^*(\mathbf{r}) \nabla^2 \psi(\mathbf{r}) d\mathbf{r}. \quad (\text{B1})$$

and electron density, defined as:

$$n(\mathbf{r}) = \psi(\mathbf{r})^* \psi(\mathbf{r}). \quad (\text{B2})$$

Taking the Laplacian on both sides:

$$\nabla^2 n(\mathbf{r}) = 2\Re \{ \psi(\mathbf{r})^* \nabla^2 \psi(\mathbf{r}) \} + |\nabla \psi(\mathbf{r})|^2 \quad (\text{B3})$$

and integrating over \mathbb{R}^3 gives

$$\begin{aligned} \int_{\mathbb{R}^3} \nabla^2 n(\mathbf{r}) d\mathbf{r} &= \int_{\mathbb{R}^3} 2\Re\{\psi^*(\mathbf{r})\nabla^2\psi(\mathbf{r})\} d\mathbf{r} \\ &\quad + 2 \int_{\mathbb{R}^3} |\nabla\psi(\mathbf{r})|^2 d\mathbf{r} \\ &= -4 \left(-\frac{1}{2} \int_{\mathbb{R}^3} \psi^*(\mathbf{r})\nabla^2\psi(\mathbf{r}) d\mathbf{r} \right) \quad (\text{B4}) \\ &\quad + 2 \int_{\mathbb{R}^3} |\nabla\psi(\mathbf{r})|^2 d\mathbf{r} \\ &= -4T + 2 \int_{\mathbb{R}^3} |\nabla\psi(\mathbf{r})|^2 d\mathbf{r}. \end{aligned}$$

Rearranging, we obtain:

$$T = \int_{\mathbb{R}^3} \left[\frac{1}{2} |\nabla\psi(\mathbf{r})|^2 - \frac{1}{4} \nabla^2 n(\mathbf{r}) \right] d\mathbf{r}. \quad (\text{B5})$$

Let us now assume a complex wave function

$$\psi(\mathbf{r}) = \sqrt{n(\mathbf{r})} e^{i\theta(\mathbf{r})}, \quad (\text{B6})$$

where $\theta(\mathbf{r})$ is the local phase.

In this form:

$$\nabla\psi(\mathbf{r}) = \frac{\nabla n(\mathbf{r})}{2\sqrt{n(\mathbf{r})}} e^{i\theta(\mathbf{r})} + i\sqrt{n(\mathbf{r})} \nabla\theta(\mathbf{r}) e^{i\theta(\mathbf{r})}, \quad (\text{B7})$$

$$|\nabla\psi(\mathbf{r})|^2 = \frac{|\nabla n(\mathbf{r})|^2}{4n(\mathbf{r})} + n(\mathbf{r}) |\nabla\theta(\mathbf{r})|^2. \quad (\text{B8})$$

Substituting (B8) into (B5) the integrand becomes

$$\tau^{\text{g-vW}}(\mathbf{r}) = \frac{|\nabla n(\mathbf{r})|^2}{8n(\mathbf{r})} + \frac{1}{2} n(\mathbf{r}) |\nabla\theta(\mathbf{r})|^2 - \frac{1}{4} \nabla^2 n(\mathbf{r}). \quad (\text{B9})$$

Generalised Kohn–Sham Kinetic Energy Density

We extend the kinetic energy decomposition to a system of N orthonormal Kohn–Sham orbitals $\psi_i(\mathbf{r})$. The total kinetic energy is

$$T = -\frac{1}{2} \sum_{i=1}^N \int_{\mathbb{R}^3} \psi_i^*(\mathbf{r}) \nabla^2 \psi_i(\mathbf{r}) d\mathbf{r}. \quad (\text{B10})$$

The total electron density is defined as

$$n(\mathbf{r}) = \sum_{i=1}^N |\psi_i(\mathbf{r})|^2. \quad (\text{B11})$$

Proceeding as in the single-orbital case and using the linearity of sums, integrals, and the Laplacian, we obtain

$$T = \int_{\mathbb{R}^3} \left[\sum_{i=1}^N \frac{1}{2} |\nabla\psi_i(\mathbf{r})|^2 - \frac{1}{4} \nabla^2 n(\mathbf{r}) \right] d\mathbf{r}. \quad (\text{B12})$$

This naturally defines the generalised Kohn–Sham kinetic energy density

$$\tau^{\text{g-KS}}(\mathbf{r}) = \sum_{i=1}^N \frac{1}{2} |\nabla\psi_i(\mathbf{r})|^2 - \frac{1}{4} \nabla^2 n(\mathbf{r}). \quad (\text{B13})$$

Complex Phase Term in Kohn-Sham DFT

For a system of N orthonormal Kohn–Sham orbitals the gradient of the phase term can be cast in terms of the current density, which is given by:

$$\mathbf{J}(\mathbf{r}) = -\frac{i}{2} \sum_k^{\text{occ}} [\psi_k^*(\mathbf{r}) \nabla\psi_k(\mathbf{r}) - \psi_k(\mathbf{r}) \nabla\psi_k^*(\mathbf{r})]$$

The gradient of the phase $|\nabla\theta(\mathbf{r})|^2$ can be related to the current density computing:

$$\begin{aligned} \mathbf{J}_\sigma(\mathbf{r}) \cdot \mathbf{J}_\sigma(\mathbf{r}) &= -\frac{1}{4} \sum_k^{\text{occ}} \left[\psi_{k\sigma}^*(\mathbf{r}) \nabla\psi_{k\sigma}(\mathbf{r}) - \psi_{k\sigma}(\mathbf{r}) \nabla\psi_{k\sigma}^*(\mathbf{r}) \right]^2 \\ &= -\frac{1}{4} \left[(\psi_{k\sigma}^*(\mathbf{r}) \nabla\psi_{k\sigma}(\mathbf{r}))^2 - (\psi_{k\sigma}(\mathbf{r}) \nabla\psi_{k\sigma}^*(\mathbf{r}))^2 \right. \\ &\quad \left. - |\psi_{k\sigma}(\mathbf{r})|^2 |\nabla\psi_{k\sigma}(\mathbf{r})|^2 \right] \end{aligned} \quad (\text{B14})$$

Assuming complex wavefunctions (B6), (B7), combining and canceling terms, this dot product yields:

$$\mathbf{J}_\sigma(\mathbf{r}) \cdot \mathbf{J}_\sigma(\mathbf{r}) = \sum_k^{\text{occ}} n_{k\sigma}^2(\mathbf{r}) |\nabla\theta_{k\sigma}(\mathbf{r})|^2. \quad (\text{B15})$$

which can be related to the gradient of the phase term [37, 38] via

$$\frac{1}{2} n_\sigma(\mathbf{r}) |\nabla\theta(\mathbf{r})|^2 = \frac{\mathbf{J}(\mathbf{r}) \cdot \mathbf{J}(\mathbf{r})}{2n_\sigma(\mathbf{r})}.$$

Scaling function

Combining the generalised von Weizsäcker and Kohn–Sham kinetic energy densities, we obtain the local scaling function

$$z_\sigma(\mathbf{r}) = \frac{\frac{|\nabla n_\sigma(\mathbf{r})|^2}{8n_\sigma(\mathbf{r})} + \frac{1}{2} n_\sigma(\mathbf{r}) |\nabla\theta_\sigma(\mathbf{r})|^2 - \frac{1}{4} \nabla^2 n_\sigma(\mathbf{r})}{\frac{1}{2} \sum_i f_{i\sigma} |\nabla\psi_{i\sigma}(\mathbf{r})|^2 - \frac{1}{4} \nabla^2 n_\sigma(\mathbf{r})} \quad (\text{B16})$$

where σ denotes a spin channel and $f_{i\sigma}$ the corresponding occupation numbers.